Examining Safe Intervention Windows for 18650 and 21700 Lithium-Ion Batteries under Heat Interruption Experiments

Wai Cheong Tam[*,†,1], Hongqiang Fang[†,1], Jian Chen[*,2], Qiuhong Wang[2], Christopher Brown[1], Md. Ismail Siddiqi Emon[1], Anthony Putorti Jr.[1]

[1]Fire Research Division, Engineering Laboratory, National Institute of Standards and Technology, Gaithersburg, Maryland, USA

[2]College of Safety Science and Engineering, Xi'an University of Science and Technology, Xi'an, China

[†]Joint first authors, [*]Corresponding authors

Abstract

This study experimentally quantifies the safe intervention window (the time between the earliest thermal runaway indicator and ignition) for cylindrical lithium-ion batteries exposed to constant external heating. A total of 77 experiments were performed on 18650 (nickel-cobalt-aluminum oxide, 3500 mAh) and 21700 (nickel-manganese-cobalt oxide, 5000 mAh) batteries using a ~ 41 W heating pad with four state of charge (SOC) conditions. When heating was terminated after safety valve breakage, ignition was preventable only within approximately 195 s to 270 s for 18650 batteries, but just about 90 s and 40 s for 21700 batteries with 25 % and 50 % SOC, respectively. At higher SOCs (75 % and 100 %), ignition occurred even when heating was stopped within 10 s and some 21700 batteries exhibited delayed ignition after a temporary cooling period of about 200 s. A joint analysis of intervention time, cutoff temperature, and temperature-rate slope identified predictive thresholds that distinguish between no-ignition and delayed-ignition outcomes. Although this study applies only to single-cell configurations under natural convection, the results provide quantitative insights that link early-stage detection to actionable response timing, providing a quantitative framework for preventing ignition in lithium-ion batteries.

Keywords: thermal runaway mitigation, intervention time, delayed ignition, lithium-ion battery safety, thermal abuse

1. Introduction

Lithium-ion (Li-ion) batteries have become indispensable for powering modern life, yet their potential to cause catastrophic fires remains a growing safety concern. In residential settings, the magnitude of this problem is alarming. In 2023 alone, the New York City Fire Department responded to 267 residential Li-ion battery fires [1], resulting in 150 injuries and 18 fatalities, which exceeds the total deaths reported in the previous two years combined. Additionally, the rate

of injury and death per incident far exceeds that of conventional home fires [2]. These statistics underscore the severity of Li-ion battery fire risks.

Thermal runaway is a rapid and self-accelerating process in which internal heating triggers exothermic reactions that release additional heat, gas, and flammable vapors. Once thermal runaway is initiated, the process can progress from initial venting (i.e., safety valve breakage) to ignition within minutes with flame jets reaching over 1000 °C and maintaining surface temperatures above 200 °C for several minutes [3]. Such extreme conditions can trigger thermal runaway propagation to nearby cells or ignite surrounding combustible materials [4]. Conventional smoke and heat detectors are not designed to detect this kind of early-stage thermal runaway [5] since initial venting and off-gassing generate minimal smoke and weak thermal signatures before ignition. As a result, ignition often occurs before any warning is signaled to occupants.

To address this limitation, the research community has developed detection systems capable of identifying the early-stage thermal runaway. Various detection parameters have been explored, including battery surface temperature [6,7], internal temperature [8,9], voltage [10,11], current [12], pressure [13,14], gaseous emissions [15-17], and ultrasonic signals [18,19]. Most recently, advancements in sensing technology have enabled detection as early as the moment the safety valve breakage [20-22] and these technologies provide valuable early warnings that could allow for timely intervention.

Despite these advancements, a major knowledge gap remains. While early detection methods continue to improve, to the best of the authors' knowledge, none of these studies [6-22] has experimentally quantified the safe intervention window after safety valve breakage. Specifically, the safe intervention window (the duration between the earliest detectable indicator such as safety valve breakage moment and the onset of ignition when external heating is interrupted) has not yet been systematically investigated.

Understanding this window is essential for designing actionable early-warning systems and safety protocols to allow sufficient time for occupants to respond effectively (i.e., whether by disconnecting power, evacuating, or activating suppression mechanisms). Therefore, this study aims to experimentally quantify the available intervention time prior to ignition for two common Li-ion batteries used in small mobility devices (18650 and 21700) across multiple states-of-charge (SOC) conditions. The results are expected to provide experimental insights for establishing safety measures that help to guide the development of effective early-warning, prevention, and mitigation systems against Li-ion battery thermal runaway.

2. Related Work

2.1 Fire Behavior and Progression of Thermal Runaway

Extensive research has been conducted to understand the fire behaviors associated with Li-ion batteries due to thermal abuse. At the battery level, many studies [23-27] have examined the various stages of thermal runaway, including the heating stage, pressure relief stage, thermal runaway stage, and weakening stage. Researchers have also investigated the underlying mechanisms governing the thermal runaway progression, such as solid electrolyte interphase decomposition [28,29], electrolyte-anode reactions [30,31], separator melting [32,33], cathode

decomposition [34,35], anode binder degradation [36,37], and electrolyte combustion [38,39]. These studies [23-27] have quantified key parameters, such as surface temperature, gaseous concentration, voltage, and pressure, for different cell configurations (i.e., size, chemistry, electrolyte composition and state-of-charge) and different applied heating power, which can be used as thresholds to quantify the various stages of thermal runaway. This body of work has provided valuable insight into how thermal runaway occurs under continuous heating without intervention. For example, when the surface temperature reaches about 168 °C and 241 °C, initial venting and ignition will occur, respectively, for 18650 lithium nickel manganese cobalt oxide batteries under an external heating of 20 W [40]. For 27100, the onset of ignition occurs when the battery surface temperature reaches approximately 189 °C [41]. However, these studies [23-41] are only based on continuous heating conditions and the thermal behavior and the potential delayed ignition after heating interruption have not been systematically investigated. Therefore, the present work aims to reveal whether thermal runaway can still occur after a temporary cooling phase and how much time is available before ignition becomes inevitable.

2.2 Prevention Strategies and Practical Limitations

Several prevention techniques have been proposed to mitigate ignition when the Li-ion battery undergoes thermal runaway process and they include air cooling, heat pipes, and immersion cooling. Among these, air cooling systems [42,43] are the most widely adopted due to their simple structure and low cost. However, their low cooling efficiency and uneven heat dissipation can result in localized hotspots which increase the risk of thermal runaway. Heat pipe systems [44,45] offer higher cooling efficiency, but their use is limited due to higher costs, structural complexity, and maintenance requirements. More recently, direct liquid immersion cooling [46,47] has emerged as a promising technique that leverages both sensible and latent heat transfer mechanisms, which offer superior cooling performance and uniform cooling. Despite their effectiveness, these advanced systems are primarily feasible for large-scale applications, such as electric vehicles and stationary energy storage systems, where space, infrastructure, and cost allow for engineered thermal management.

In contrast, small personal mobility devices and consumer electronics generally lack the capacity to incorporate such advanced cooling architectures. They rely almost entirely on passive heat dissipation through natural convection which may be insufficient once the battery begins to overheat. This raises another critical question: when overheating occurs, will disconnecting the power source responsible for the overheating be enough to prevent the ignition and, if so, how much time is available for safe intervention? Existing studies have primarily focused on continuous heating conditions; therefore, there remains a need to understand the thermal behavior of batteries under interrupted heating and to examine whether stopping the heat source alone can effectively prevent ignition once the battery enters the early-stage thermal runaway.

This study addresses the above research gap through a systematic experimental investigation of Li-ion battery behavior under constant external heating and subsequent heating interruption. The key contributions are as follows:

1. To provide detailed thermocouple measurements from two series of experiments involving constant external heating (≈ 41 W) for two different types of batteries (18650 NCA and

21700 NMC) at four different state-of-charge conditions (100 %, 75 %, 50 %, and 25 %) and various heating interruption times.

2. To experimentally determine the available time window for safe intervention for both 18650 NCA and 21700 NMC batteries across multiple states-of-charge.
3. To examine temperature behaviors associated with delayed ignition and to characterize the corresponding parameters, such as time-to-event, temperature, and rate of change of temperature.

The findings from this study will help identify the safe intervention time, establish thresholds to quantify the delay in ignition after heating is stopped, and its behavior, which will be important for the development of effective response strategies, such as power disconnection, evacuation, or fire suppression.

3. Methodology

3.1 Experimental Setup

Figure 1a shows the overall view of the experimental setup. The setup consisted of an open-top enclosure with nominal dimensions of 2.4 m × 2.4 m × 2.4 m and an approximately 0.5 m-wide door opening. The enclosure frame was constructed from metal wall studs (6 cm × 3.2 cm) and enclosed with lightweight drywall panels, perforated metal sheets, and thin plexiglass walls. The top of the enclosure was covered by a metal mesh screen to prevent flaming debris from escaping while allowing adequate ventilation. The enclosure was located at the center of a 5 MW exhaust hood (6.1 m × 6.1 m) operating at an airflow rate of approximately 3.2 kg/s. Also, there were two 110/24-32 power converters and one data acquisition display located near the testing area. The power converters supplied a regulated 28 VDC output to the heating element (see below for descriptions) and the display provided real-time temperature monitoring.

Figure 1b presents a front view of the setup showing a wooden battery fixture and a detector array positioned inside the enclosure. The battery rack could accommodate up to eight batteries at a time and it was mounted approximately 76 cm from the front plexiglass wall and approximately 74 cm above the floor which is roughly equivalent to standard table height. The detector array included two smoke/CO detectors, two heat detectors, and two explosive gas detectors. A video camera and an infrared camera were located outside of the enclosure and they were used to continuously capture thermal and visual data throughout each experiment. This configuration allows real-time monitoring of temperature distribution, ignition, and flame development during the experiments.

3.2 Li-ion Batteries with Heating Element and Temperature Measurement

Figures 1c and 1d show the thermal abuse configuration for the 18650 NCA and 21700 NMC Li-ion batteries, respectively, each equipped with a heating element (flexible heat pad) and thermocouple. The 18650 NCA battery (see Fig. 1c) has a nominal voltage of 3.7 V and a capacity of 3500 mAh, with a lithium nickel cobalt aluminum oxide (NCA) cathode and a graphite anode. The 21700 NMC battery (see Fig. 1d) has the same nominal voltage (3.7 V) and a nominal capacity

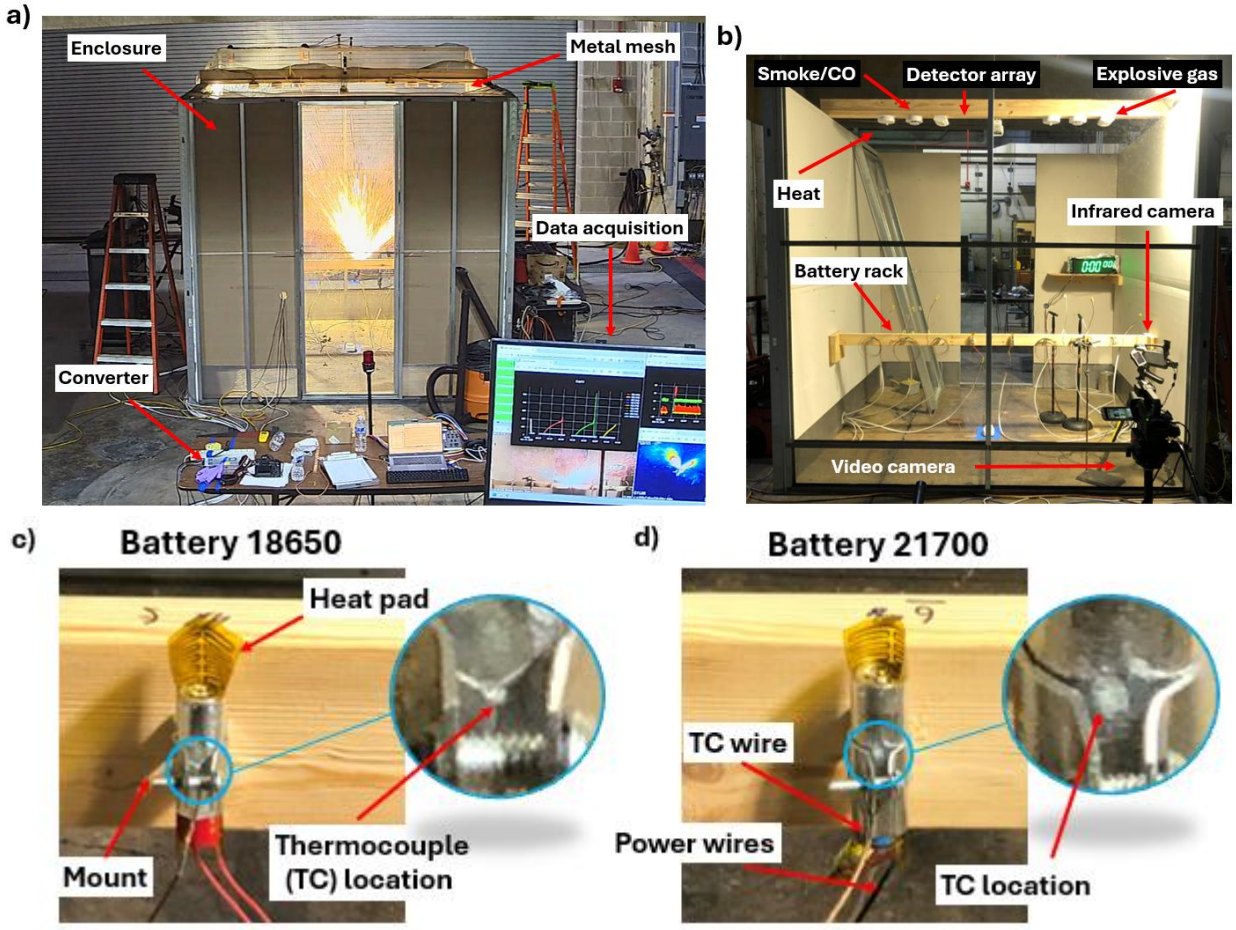

Figure 1. a) Overall view, b) front view of the experimental setup, and zoom-in view of c) 18650 and d) 21700 Li-ion battery with the thermal abuse setup and thermocouple measurement location.

of 5000 mAh using lithium nickel manganese cobalt oxide (NMC) as the cathode and graphite as the anode.

Prior to testing, all batteries were conditioned to the desired state-of-charge using a three-cycle constant-current/constant-voltage protocol [22,23]. Each battery was discharged to 2.5 V at 0.2 C, then charged to 4.2 V at the same current. The constant-voltage step continued until the current decreased to 160 mA, followed by a one-hour rest period between cycles to ensure electrochemical stability. After the final charge, the cells were rested for 24 hours before testing. Table 1 summarizes the key parameters of both batteries.

As shown in Figs. 1c and 1d, a flexible silicone heating pad with nominal dimensions of 100 mm × 40 mm × 0.25 mm was attached to the surface of each battery with the first resistive coil located near the cell's lower end to ensure consistent placement. The 18650 NCA and 21700 NMC cells occupy approximately 70 % and 80 % of the total heating area, respectively. The heating pad had a resistance of 19.1 Ω ± 0.2 Ω. Powered by a voltage input of 28.0 V ± 0.1 V from the power converter shown in Fig. 1a, an electric power of 41 W ± 0.4 W was delivered. The electric power

Table 1. Summary of key parameters for the 18650 and 21700 batteries.

Name	Unit	18650	21700
Cathode	–	Lithium nickel cobalt aluminum oxide (NCA)	Lithium nickel manganese cobalt oxide (NMC)
Anode	–	Graphite	Graphite
Dimension (diameter × height)	mm × mm	18 × 650	21 × 700
Nominal capacity	mAh	3500	5000
Nominal voltage	V	3.7	3.7
Maximum cut-off voltage	V	4.2	4.2
Minimum cut-off voltage	V	2.5	2.5
Mass	g	48.2 ± 0.3	68.7 ± 0.5
State of charge	%	25, 50, 75, 100	25, 50, 75, 100

was selected to produce a maximum temperature of approximately 250 °C to trigger thermal runaway. The heating pad was secured to the battery surface using an adhesive to ensure full thermal contact. A thermocouple[1] was positioned at the midpoint of the battery using high-temperature tape to measure the surface temperature. It should be noted that the thermocouples were not covered by the heating pad and temperature data were collected at a sampling frequency of 1 Hz.

3.3 Experimental Procedures

Each experiment began by applying constant power to the heating pad until the battery reached a surface temperature sufficient to induce safety valve breakage (SVB) and then ignition. Time stamps for the start of heating, safety valve breakage, and ignition were marked during the experiment. Two series of experiments were conducted:

1. Continuous heating experiments in which heating continued until ignition occurred to determine the time interval between SVB and ignition,

2. Interrupted heating experiments in which heating was stopped at various times after SVB to evaluate the safe intervention window and delayed ignition behavior. The time intervals obtained from the first series of experiments were used to determine the heating stop time in the second series of experiments.

In total, 77 experiments were carried out and the complete test matrix for the two series of experiments and the heating stop time are provided in Appendix A.

3.4 Seek-and-Wait Approach

[1] Type K, bare bead, 24 American Wire Gauge (AWG) thermocouples (TC) with a temperature range up to 1250 °C with a standard relative uncertainty value of ± 0.75 %, as reported by the manufacturer, were used for these experiments.

The heating interruption time was determined based on the interval between SVB and ignition (defined as the Delay Time). The initial heating stop time was set to approximately half of the Delay Time. For example, for 18650 batteries at 100 % SOC, the average times to SVB and ignition were 285 s and 513.5 s, respectively, resulting in an initial heating stop time of 120 s. If ignition was not observed, the heating stop time was increased by approximately half of the initial value. Conversely, if ignition still did not occur under adjusted conditions, the heating stop time was decreased by a similar margin. This iterative process continued until delayed ignition was observed. Once delayed ignition was identified, repeated experiments were conducted to confirm reproducibility. Subsequently, the heating stop time was reduced in increments of approximately 5 s to 15 s to determine the time below which delayed ignition no longer occurred. For 18650 batteries at 100 % SOC, the evaluated heating stop times were 120 s, 180 s, 210 s, 195 s, 200 s (first delayed ignition observed), 200 s (delayed ignition confirmed), 193 s, and 185 s (no ignition).

4. Results and Discussion

4.1 Continuous Heating Experiments

A total of 26 continuous heating experiments were conducted (14 for 18650 NCA batteries and 12 for 21700 NMC batteries) to quantify the time interval between SVB and ignition (i.e., thermal runway). Each SOC condition was repeated at least three times to obtain averaged values. Two selected continuous heating experiments are provided in Video S1 and Video S2 in the supplementary materials.

Figure 2a shows the selected surface temperature profiles for the 18650 NCA batteries at four SOC conditions, including a zoomed-in view of the SVB event. The temperature profiles exhibit a clear dependence on SOC. Batteries with higher SOCs reached ignition more rapidly. Also, the onset ignition temperature increased as SOC decreased which indicates that batteries at lower SOC require greater thermal input to reach ignition. For SVB, the zoomed-in plot shows that a noticeable temperature drop at the moment of SVB is observed in the 25 % SOC case, although this effect is minimal at higher SOCs. The corresponding SVB time and temperature are provided in Table 2. It should also be noted that the maximum surface temperature could not be recorded for the 100 % and 25 % SOC cases because the batteries experienced either deflagration or ejection

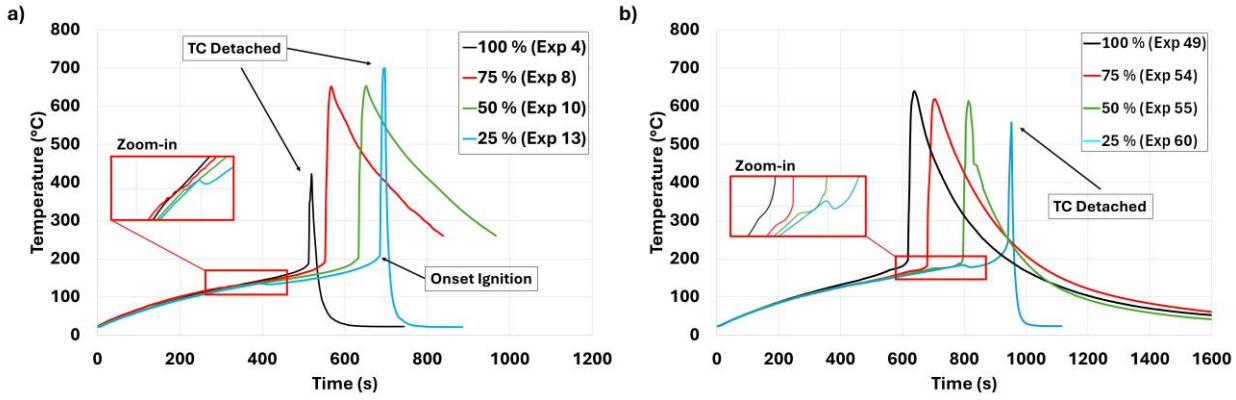

Figure 2. Selected surface temperature profiles for a) 18650 batteries and b) 21700 batteries.

during ignition. As a result, the complete relationship between temperature and SOC could not be established in this study. However, published data [23] generally report that the maximum surface temperature increases with increasing SOC.

Figure 2b shows the corresponding results for 21700 NMC batteries. It can be seen that lower SOCs also resulted in longer time to ignition and higher onset ignition temperature. In terms of peak temperature, the value generally increased with higher SOCs. For SVB, there are four important observations: i) the time required to reach SVB increased as SOC decreased, ii) the SVB temperature increased with decreasing SOC, iii) there was a temporary temperature change immediately after SVB and the temperature change was more pronounced at lower SOCs (i.e., a temperature drop of 6 °C at 25 % SOC), and iv) the delay time between SVB and ignition was significantly shorter at higher SOC conditions. Additional quantitative comparisons are shown in Table 2.

Table 2 summarizes the average values with standard deviations for both 18650 NCA and 21700 NMC batteries across four SOC conditions: 1) time to SVB, 2) SVB temperature, 3) time to ignition, 4) ignition temperature, 5) the SVB-to-ignition time delay, and 6) the associated temperature difference between SVB and ignition temperatures. For 18650 NCA cells, it can be observed that the SVB temperature ranged from approximately 110 °C to 130 °C, while the onset ignition temperature ranged from 183 °C to 208 °C. With the exception of the 100 % SOC case for the time to SVB and SVB temperature, all six averaged quantities increased as the SOCs decreased. For the 21700 NMC cells, SVB temperatures were generally 50 °C higher than those of the 18650 NCA cells, ranging from 162 °C to 177 °C, and the time to SVB was roughly twice as long. However, the 21700 NMC cells exhibited a much shorter transition from SVB to ignition. At 100 % SOC, for example, ignition occurred only 66.3 s ± 2.2 s after SVB. This observation indicates that although the larger NMC cells required more time to reach ignition, it progressed more rapidly once SVB occurred.

The delay times obtained from these continuous heating experiments served as reference values for the interrupted heating experiments described in Section 4.2, where the possibility of preventing ignition by stopping external heating was investigated.

Table 2. Summary of average quantities for 18650 and 21700 batteries in the continuous heating experiments.

	SOC	SVB Time	SVB Temperature	Onset Ignition Time	Onset Ignition Temperature	Delay Time	Temperature Difference
	(%)	(s)	(°C)	(s)	(°C)	(s)	(°C)
18650	**100**	285.0 ± 0.0	117.6 ± 1.1	513.5 ± 4.5	186.9 ± 0.5	228.5 ± 4.5	69.3 ± 0.6
	75	274.0 ± 15.9	110.4 ± 4.2	549.7 ± 14.6	183.4 ± 1.5	275.7 ± 16.5	73.0 ± 5.2
	50	333.0 ± 12.8	121.8 ± 3.4	641.3 ± 6.1	200.2 ± 1.6	308.3 ± 18.6	78.5 ± 1.9
	25	377.5 ± 9.5	129.9 ± 2.2	689.5 ± 0.5	208.1 ± 0.7	312.0 ± 9.0	78.2 ± 1.6
21700	**100**	549.0 ± 6.7	161.8 ± 1.7	615.3 ± 6.1	192 ± 2.9	66.3 ± 2.2	30.1 ± 2.2
	75	616.0 ± 10.1	162.6 ± 1.7	690.3 ± 12.4	184.9 ± 3.3	74.3 ± 2.6	22.4 ± 3.3
	50	682.7 ± 5.6	169.6 ± 6.2	782.3 ± 5.8	189.7 ± 8.5	99.7 ± 6.3	20.1 ± 2.4
	25	789.7 ± 10.1	176.7 ± 7.6	936.0 ± 0.0	227.7 ± 22.8	148.3 ± 8.0	51.0 ± 15.5

4.2 Interrupted Heating Experiments

In this series, the heating was intentionally stopped after SVB to identify the maximum intervention time at which ignition could still be prevented. The time-to-stop-heating was selected using then seek-and-wait approach based on the average delay time obtained from the continuous heating experiments. Each experiment was repeated to determine repeatability, especially when delayed ignition occurred after heating termination. A total of 51 interrupted heating experiments (29 for 18650 NCA cells and 22 for 21700 NMC cells) were conducted. Two selected cases, Video S3 and Video S4, are provided in the supplementary materials.

4.2.1 Temperature behaviors for 18650 NCA batteries

Figure 3 shows the surface temperature profiles relative to 10 s before the SVB moment for the 18650 NCA batteries under four SOC conditions. Each profile, except for the no ignition case, is plotted up to one second before ignition. Three temperature profiles are shown in each figure (see Fig. 3a): dotted lines represent ignition, solid lines represent delayed ignition, and long dashed lines represent no ignition. Note that the heat intervention times for all experiments are provided in Appendix A.

For delayed ignition cases, after heating was stopped, the increasing trend of the surface temperature changed. In some cases (i.e., 50 % SOC in Fig. 3c and 25 % SOC in Fig. 3d), the temperature rise slowed but continued to increase; in others (i.e., 100 % in Fig. 3a and 75 % in

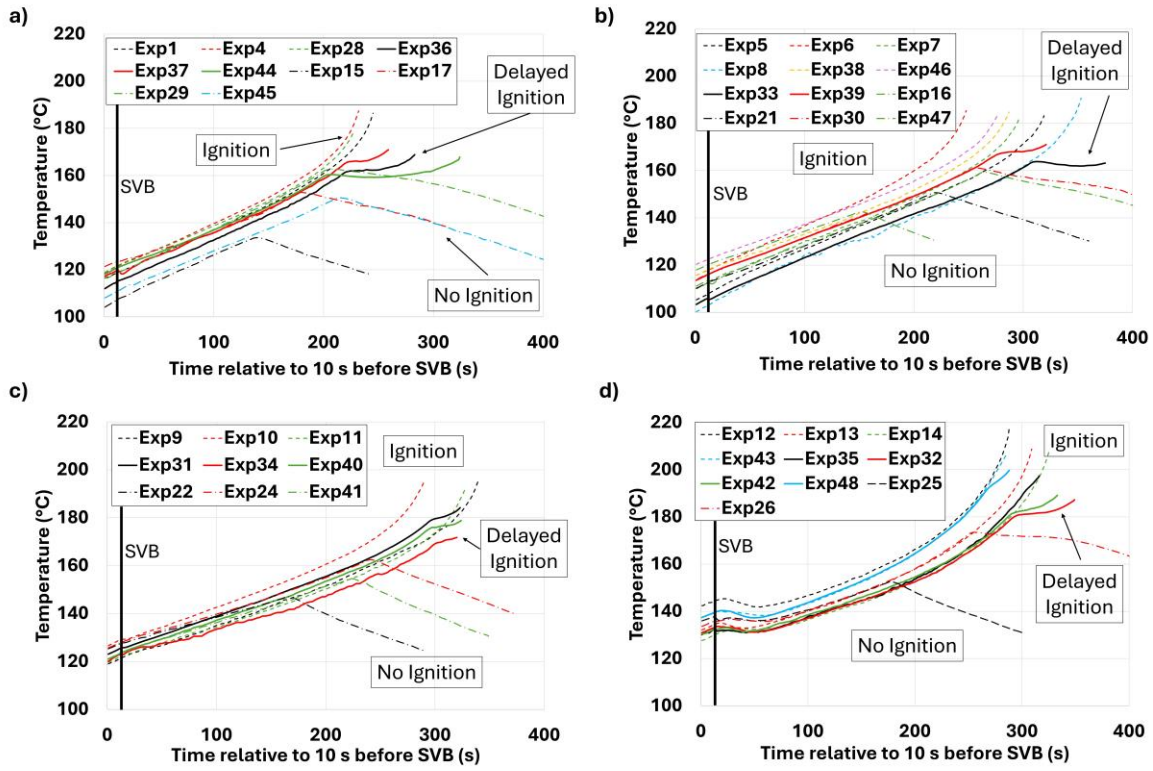

Figure 3. Temperature profiles of no ignition, delayed ignition, and ignition for 18650 batteries with a) 100 %, b) 75 %, c) 50 %, and d) 25 % SOC conditions.

Fig. 3b), a slight cooling was observed. However, after a certain duration, a temperature increase occurred and then accelerated exponentially until the onset of ignition. For ignition cases, the surface temperature continuously increased even heating was stopped and thermal runaway progressed. In contrast, for no ignition cases, the surface temperature decreased almost linearly after heating was stopped, signifying the absence of sustained internal reactions. More in-depth analyses and discussions are provided in Section 4.4.

The observed temperature responses can be interpreted from a thermochemical perspective. After SVB, the temperature profile is governed by the energy balance between internal heat generation and external heat dissipation. The internal heat generation arises from exothermic reactions, such as solid electrolyte interphase decomposition, anode-electrolyte reactions, and cathode decomposition. These reactions are highly temperature-dependent and can result in accelerated heat release once a critical temperature is reached.

For delayed ignition cases, the temporary cooling after heating termination indicates that heat dissipation initially exceeds heat generation. However, as temperature remains sufficiently high, ongoing exothermic reactions progressively intensify, eventually leading to a net heat gain and renewed temperature rise to cause ignition. In contrast, for no ignition cases, the internal heat generation is insufficient to overcome heat losses which leads to continuous cooling.

4.2.2 Temperature behaviors for 21700 NMC cells

Figure 4 shows the corresponding surface temperature profiles for 21700 NMC batteries. While the ignition and no-ignition profiles followed similar patterns to those of 18650 NCA batteries, the delayed ignition behavior differed substantially. At 100 % SOC, the temperature exhibited a modest fluctuation of 1 °C to 3 °C in approximately 40 s after heating stopped. At 75 % and 50 % SOC, the temperature variations were more pronounced. For example, in Experiment 81 (Fig. 4b), the surface temperature decreased from approximately 170 °C to 155 °C in about 160 s, then gradually rose to ignition. At 25 % SOC, two distinct cooling phases were observed (Fig. 4d). The initial drop was due to SVB and the secondary decline was due to heating termination. It is believed that the delayed ignition was likely attributed to the energy imbalance (net gain) in heat gain from internal reactions and heat dissipation through natural convection.

The results suggest a safety implication: a temporary temperature decline after heating termination does not guarantee thermal stability. Instead, the persisting internal exothermic reactions can eventually reverse the cooling trend, leading to ignition after a delay. This effect was more pronounced in the investigated 21700 NMC batteries, indicating that the larger in size and the difference in NMC cathode may lead to stronger self-heating potential due to the greater thermal and chemical inertia, respectively.

The dependence on SOC can be explained by the availability of reactive species and the amount of electrochemical energy. At higher SOC levels, the anode is likely to be in a more lithiated state while the cathode is in a more oxidized and less thermally stable state. These conditions increase both the likelihood and intensity of exothermic reactions. In particular, cathode decomposition at elevated temperatures can release oxygen which promotes electrolyte oxidation and significantly enhances heat generation. In contrast, at lower SOC levels, the anode contains less intercalated lithium and the cathode remains relatively more stable. As a result, the exothermic reaction

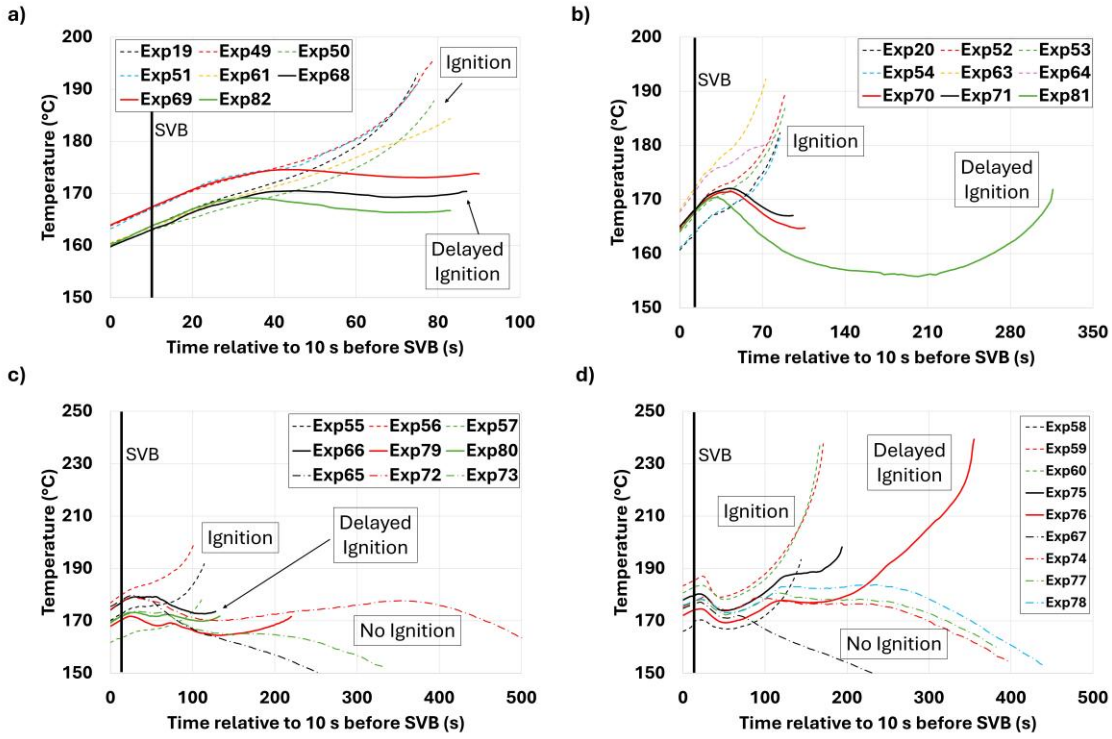

Figure 4. Temperature profiles of no ignition, delayed ignition, and ignition for 21700 batteries with a) 100 %, b) 75 %, c) 50 %, and d) 25 % SOC conditions.

pathways are reduced, leading to lower total heat release. Under these conditions, if heat dissipation exceeds internal heat generation, the battery temperature decreases and ignition is avoided.

4.3 Safe Intervention Window

Figure 5a shows the ignition risk associated with 18650 NCA batteries for different intervention times relative to SVB across four SOC conditions. There were three safe post-heating outcomes: i) no ignition, where heating was stopped and no ignition occurred (shown in blue bar); ii) delayed ignition, where temperature initially decreased but later rose due to self-heating, leading to ignition (black bar); and iii) ignition, where temperature continued to rise until ignition occurred (red bar).

For the 18650 NCA batteries, the maximum safe intervention window ranged approximately from 195 s to 270 s depending on the SOC conditions. In general, the maximum safe intervention window time decreased as SOC decreased, with the exception of the 100 % SOC condition, which exhibited a safe intervention time of about 195 s. An overlap region exists between the no ignition and delayed ignition outcomes, particularly at 100 % and 75 % SOC. This overlapping behavior indicates that the battery was in a critical thermal condition where small variations in temperature or reaction kinetics can significantly influence the outcome. For that, identical intervention times can result in different outcomes, indicating that intervention time alone is insufficient to define the ignition outcome. The effect of other parameters, such as temperature at the moment of interruption, on the delayed ignition behavior is presented in Section 4.4.

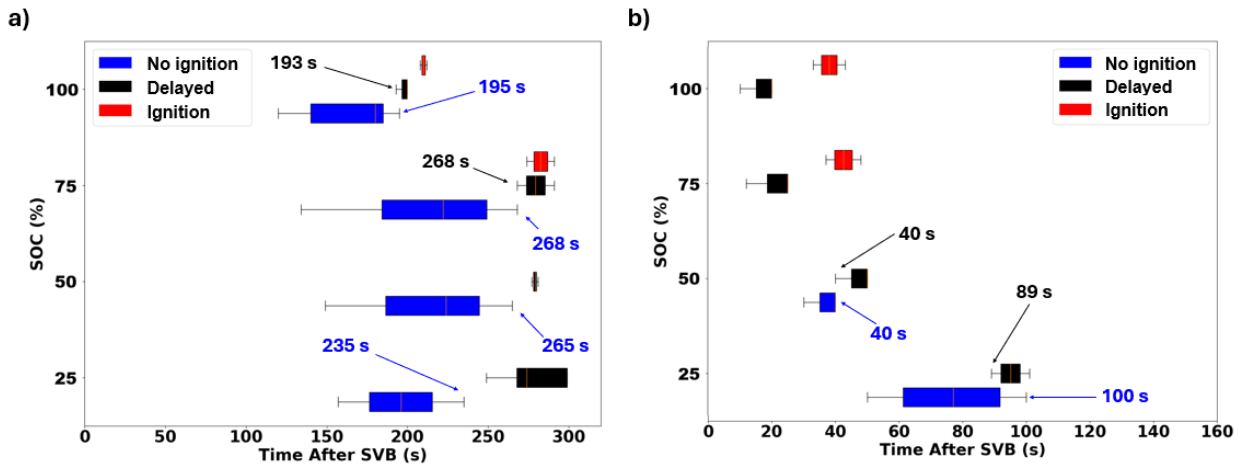

Figure 5. The relationship of ignition risk and time after SVB and the safe intervention time for a) 16850 batteries and b) 21700 batteries.

Figure 5b shows the corresponding results for 21700 NMC batteries. Compared with 18650 NCA batteries, the safe intervention window was significantly smaller. At 25 % SOC, ignition could be prevented only when heating was stopped within about 85 s and the window decreased to about 40 s for 50 % SOC. Also, results show that the overlap region between no ignition and delayed ignition was broader. At 25 % SOC, the overlapping region was about 10 s. In addition, at high SOC conditions, ignition was not preventable. For example, at 100 % and 75 % SOCs, the data show that delayed ignition occurred even when heating was stopped within 10 s after SVB. The shorter intervention window observed in 21700 NMC batteries can be attributed to both material chemistry and battery geometry. NMC cathodes generally have lower thermal stability than NCA with earlier onset of decomposition and oxygen release, which enhances exothermic reactions. In addition, the larger battery size increases the thermal mass and reduces the surface-area-to-volume ratio. These attributions promote heat accumulation and limit the heat dissipation. For that, the likelihood of sustained self-heating is greatly increased even after external heating is stopped.

4.4 Effect of Temperature, Delayed Ignition Time, and Temperature Rate

4.4.1 Battery surface temperature at heating interruption

To further investigate the conditions that govern delayed ignition, additional analysis was conducted using the interrupted heating data. Fig. 6a plots the surface temperature of the 18650 NCA batteries at the moment when heating was stopped against the intervention time relative to SVB. Each data point corresponds to a single experiment and is classified as either no ignition, delayed ignition, or ignition. The distribution of points shows three outcome regions.

A no ignition region is observed when the surface temperature at interruption is below 160 °C and the heating duration after SVB is less than 160 s. Under these conditions, the heat generated by internal reactions is insufficient to overcome natural convection and so ignition can be prevented. Conversely, an ignition region appears when the temperature exceeds 170 °C and the intervention time is longer than 270 s, resulting in either delayed ignition or ignition. Between these two regions lies a possible ignition region where the outcome is probabilistic. In the possible ignition region,

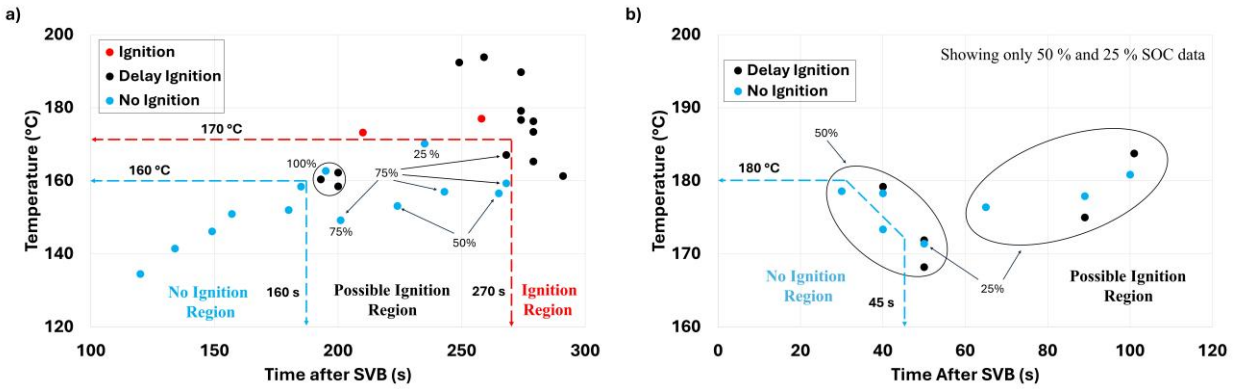

Figure 6. Relationship between surface temperature at heating interruption and intervention time after SVB for (a) 18650 and (b) 21700 batteries.

some batteries stabilized while others ignited. This observation suggests that ignition probability was likely affected by the temperature at the moment when heating was stopped.

Figure 6b shows the same analysis for 21700 NMC batteries at 50 % and 25 % SOC. In contrast to the 18650 NCA batteries, the no ignition region is substantially smaller and the possible ignition region is widely distributed throughout the rest of the data domain. It can be seen that ignition can be prevented only if the surface temperature is below 180 °C and the post-SVB heating duration is less than 30 s, or when the temperature is below 175 °C with heating terminated within 45 s. Outside these limits, delayed ignition or ignition is likely to occur. It should be noted that data for 100 % and 75 % SOC are not plotted in Fig. 7b because even when heating was stopped at about 10 s, delayed ignition occurs. For that, the no-ignition region was not presented for high SOC conditions.

4.4.2 Delayed ignition time as a function of surface temperature

Figure 7a shows the relationship between surface temperature at heat interruption and the time to delayed ignition relative to the moment of heat intervention for the 18650 NCA batteries at four SOC levels. Systematic trends are observed. Higher SOC batteries generally require lower temperatures to trigger delayed ignition. The average temperatures associated with delayed ignition were approximately 158 °C, 164 °C, 170 °C, and 183 °C for 100 %, 75 %, 50 %, and 25 % SOC, respectively. In addition, lower surface temperatures corresponded to longer times to yield delayed ignition, whereas higher temperatures yielded much shorter delays. For example, at 100 % SOC, the battery takes about 129 s to reach delayed ignition when the surface battery is about 158 °C. When the temperature is higher (i.e., at about 162 °C), about 49 s is needed to reach delayed ignition. This behavior is consistent for four different SOCs.

Figure 7b shows the corresponding results for 21700 NMC batteries. The same trend of decreasing temperature with increasing SOC is observed. However, depending on the SOC condition, the time to ignition was more sensitive to the surface temperature. For example, with an SOC of 75 % or below, the time to delayed ignition ranged from approximately 75 s to 240 s. Compared with 16850 batteries, the delayed ignition time was about twice as long. Taking the temperature profile from

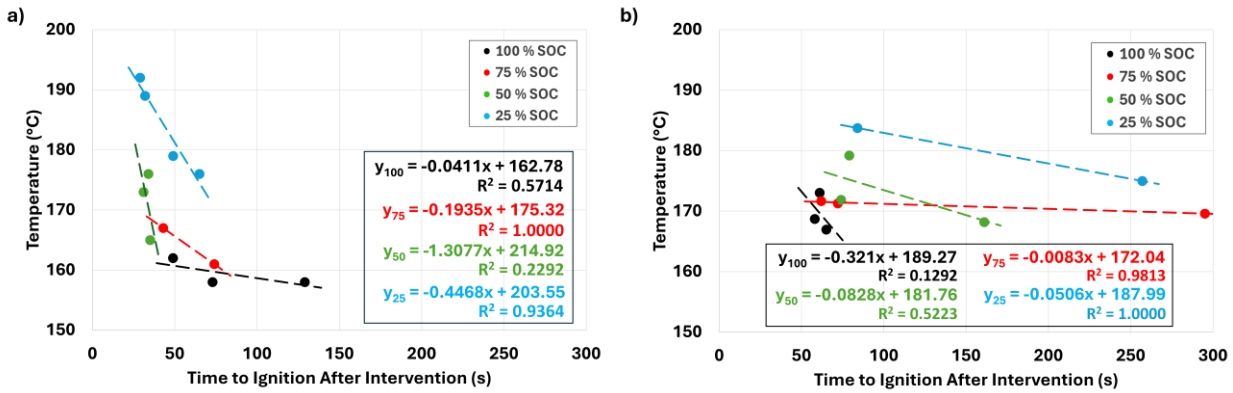

Figure 7. Delayed ignition as a function of temperature and time to ignition after intervention a) 18650 batteries and b) 21700 batteries.

Exp 81 in Fig. 4b, where 21700 NMC batteries can exhibit prolonged cooling before reheating to reach ignition, this behavior creates a false sense of stability if judged solely by short-term temperature behavior.

4.4.3 Effect of temperature rate

The rate of change of surface temperature was also analyzed to distinguish ignition, delayed ignition, and no ignition outcomes. Fig. 8a and 8b show the temperature rate profiles of two selected cases, 100 % and 25 % SOC, respectively, for 18650 NCA batteries. For delayed ignition cases, the temperature rate decreased after heating stopped but remained positive and began to rise again approximately 30 s to 50 s before ignition. For no ignition cases, the temperature rate remained negative throughout, indicating a monotonic cooling trend. For ignition cases, the temperature rate increased exponentially until ignition occurred.

Figures 8c and 8d present the corresponding results for 21700 NMC batteries at 50 % and 25 % SOC. While delayed ignition and ignition cases followed patterns similar to those of 18650 NCA batteries, a key difference is observed in the no-ignition cases. The data showed that there was a temporary rebound in temperature rate after heating was stopped. However, the rate never recovered to a level sufficient to sustain self-heating and eventually transitioned into the negative region. For example, at 50 % SOC, the temperature rate fluctuated at around 0.05 °C/s after heating intervention and did not exceed 0.06 °C/s for Exp 72. This observation suggests that the rate of change of temperature can serve as a parameter for assessing ignition risk. A negative and steadily decreasing temperature rate indicates safe decay, whereas a reversal from negative to positive could signal the onset of self-heating, potentially leading to delayed ignition.

4.5 Summary of Quantitative Thresholds for Ignition Prevention

Table 3 summarizes experimentally derived thresholds for the key parameters for safe intervention for both battery cells under different SOC conditions based on constant heating of about 41 W. There are three parameters and they are the latest safe intervention time, surface temperature at the moment of heat intervention, and the rate of change of temperature after heat intervention. The latest safe intervention time relative to SVB is selected to be the latest heat stopping time that does

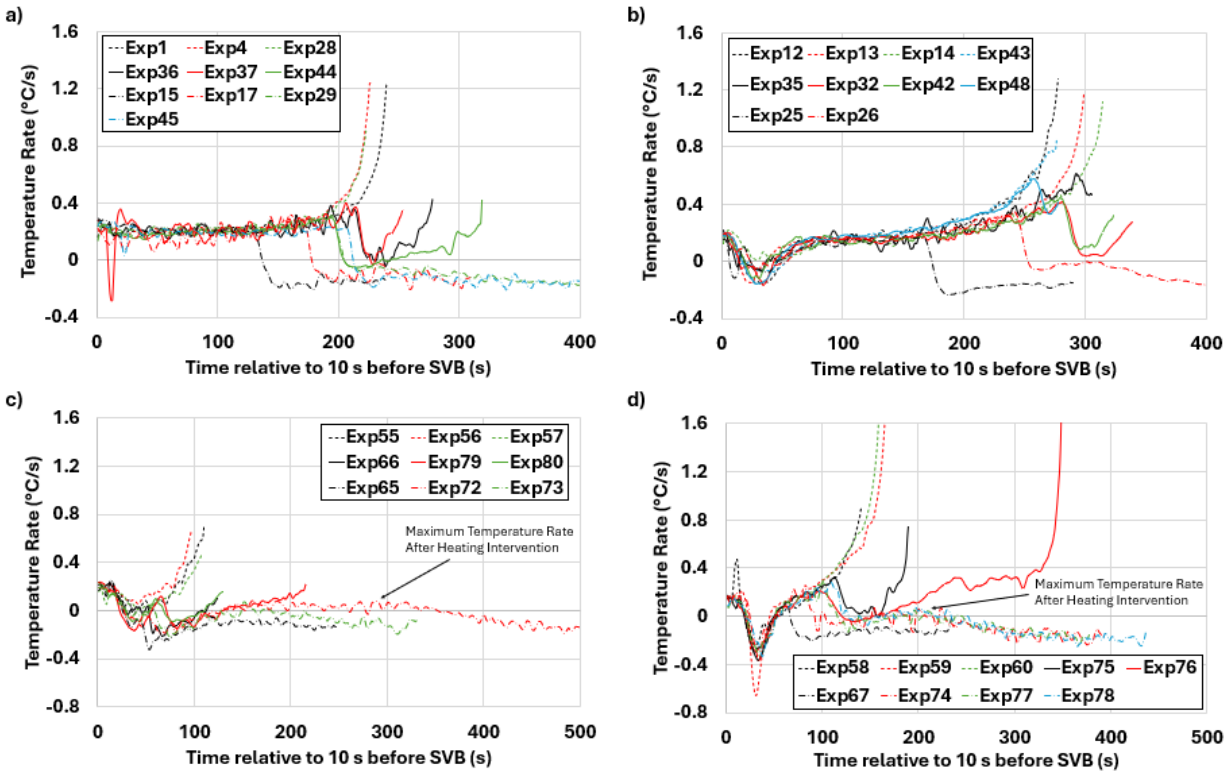

Figure 8. Rate of change of temperature over time for a) 18650 100 % SOC, b) 18650 25 % SOC, c) 21700 50 % SOC, and d) 21700 25 % SOC.

not lead to no ignition (see Figure 5). It should be noted that since delayed ignition occurs for both 100 % and 75 % SOC for 21700 batteries even when heating is stopped within 10 s and 12 s, respectively, ignition prevention parameters are not available. For surface temperature at the moment of heat intervention and the rate of change of temperature after heat intervention, they are obtained from the no ignition cases. The reported values are the mean quantities and the standard deviations are also provided.

Table 3. Summary of ignition prevention parameters.

	State-of-Charge	Latest Safe Intervention Time Relative to SVB	Temperature at Intervention	Temperature Rate of Change after Intervention
	(%)	(s)	(°C)	(°C/s)
18650	**100**	193	151.9 ± 10.7	-0.06 ± 0.03
	75	268	151.8 ± 7.0	-0.09 ± 0.05
	50	265	151.9 ± 4.3	-0.15 ± 0.01
	25	235	160.6 ± 9.6	-0.08 ± 0.08
21700	**50**	40	172.5 ± 2.8	0.02 ± 0.07
	25	89	176.6 ± 2.9	0.02 ± 0.06

In general, the values in Table 3 provide data-driven insights for estimating whether ignition can be avoided once external heating is interrupted. For example, for 18650 NCA batteries with 100 % SOC, if the safe intervention time is less than about 193 s, the intervention surface temperature is less than about 152 °C, and the rate of change of temperature is less than about - 0.06 °C/s, it is likely that the batteries will not lead to delayed ignition or ignition. However, when the thresholds exceed those values, the likelihood of delayed ignition or ignition increases.

It should be noted that these thresholds are not universal, as they are derived under specific experimental conditions and do not represent all scenarios. However, they provide the quantitative framework for determining whether heating interruption alone is sufficient to prevent ignition and for assessing the residual risk once early indicators of thermal runaway have appeared.

Conclusion

This study experimentally quantified the safe intervention window between safety valve breakage and ignition in two common cylindrical Li-ion battery cells (18650 NCA and 21700 NMC) with different state-of-charge (SOC) conditions under a constant heating of about 41 W. A total of 77 single-battery experiments, including both continuous heating and interrupted heating scenarios, were conducted to characterize time-to-ignition, delayed ignition behavior, and intervention thresholds. There are four findings: 1) quantified safe intervention windows, 2) delayed ignition behaviors, 3) influence of battery chemistries and SOC, and 4) quantitative thresholds for ignition prevention.

1. For 18650 NCA cells, the available intervention time ranged from 200 s to 275 s depending on the SOC. For 21700 NMC cells, this window decreased to about 85 s at 25 % SOC and 40 s at 50 % SOC. At higher SOC (75 % and 100 %), ignition occurred even when heating was stopped within 10 s after safety valve breakage.

2. Both battery cells exhibited delayed ignition, characterized by temporary surface cooling followed by a renewed temperature rise and subsequent ignition. This suggests that transient cooling does not imply internal stability, as residual exothermic reactions can persist.

3. The chemistry and the size of the battery play important roles to yield greater thermal and chemical inertia and stronger self-heating effects, underscoring that geometry, mass, and battery chemistry significantly affect thermal runaway dynamics. Lower state-of-charge did not always ensure safety.

4. Quantitative thresholds for safe intervention were derived under the conditions investigated. For example, ignition for 18650 NCA batteries at 100 % SOC could be preventable if heating was stopped in less than about 193 s with the intervention occurred below approximately 152 °C and the post-cutoff change of temperature rate was less than - 0.06 °C/s.

Although these findings are not universal and are specifically limited to the experimental configurations in this study, they provide insights for linking early detection to actionable response time, bridging a knowledge gap between thermal runaway sensing research and fire safety planning.

Recommendations and Future Work

The results are bounded by single-cell coupled configurations, one abuse mode (constant external heating), and constant natural convection. Future studies should investigate the delayed ignition behaviors separating the effect of battery size and chemistry (i.e., 18650 with NCA batteries vs 18650 NMC batteries and 21700 with NCA batteries vs 21700 NMC batteries) with different power settings because the delayed ignition behaviors are likely functions of battery size, chemistry, and heating rate. Additional studies are also needed to explore various intervention strategies (i.e., active cooling, venting, or suppression) that can be triggered within the quantified window. Further research on battery packs and modules is also essential to account for cell-to-cell interactions and propagation effects. These insights will help optimize early-warning algorithms and practical fire-safety systems for residential and industrial applications.

References

[1] Adams, E., and Kavanagh, L., 2023. Annal Report. Bureau of Fire Investigation, Investigative Management and Reporting System, Fire Department - City of New York. New York. https://www.nyc.gov/assets/fdny/downloads/pdf/about/bfi_2023_annual_report.pdf (Accessed on March 25, 2026).

[2] Hall, S., and McGree, T., 2025. Home Structure Fires. National Fire Protection Association Journal on Emerging Issues. National Fire Protection Association. Quincy, Massachusetts.

[3] Tang, W., Tam, W.C., Yuan, L., Dubaniewicz, T., Thomas, R. and Soles, J., 2020. Estimation of the critical external heat leading to the failure of lithium-ion batteries. *Applied thermal engineering*, *179*, p.115665.

[4] Mallick, S. and Gayen, D., 2023. Thermal behaviour and thermal runaway propagation in lithium-ion battery systems–A critical review. *Journal of Energy Storage*, *62*, p.106894.

[5] Dahlbom, S., Sanfridson, M. and Sjöblom, T., 2023. Evaluation of Detection Principles and Challenges in Early Detection of Thermal Runaway in Batteries. RISE Research Institutes of Sweden. Internal Report IR09.15.

[6] Raijmakers, L.H.J., Danilov, D.L., Eichel, R.A. and Notten, P.H.L., 2019. A review on various temperature-indication methods for Li-ion batteries. *Applied energy*, *240*, pp.918-945.

[7] Yu, Y., Vergori, E., Worwood, D., Tripathy, Y., Guo, Y., Somá, A., Greenwood, D. and Marco, J., 2021. Distributed thermal monitoring of lithium ion batteries with optical fibre sensors. *Journal of Energy Storage*, *39*, p.102560.

[8] Zhu, S., Han, J., An, H.Y., Pan, T.S., Wei, Y.M., Song, W.L., Chen, H.S. and Fang, D., 2020. A novel embedded method for in-situ measuring internal multi-point temperatures of lithium ion batteries. *Journal of power sources*, *456*, p.227981.

[9] Jiang, J., Chen, X., Niu, Y., He, X.R., Hu, Y.L. and Wang, C., 2022. Advances in flexible sensors with MXene materials. *New Carbon Materials*, *37*(2), pp.303-320.

[10] Kang, Y., Duan, B., Zhou, Z., Shang, Y. and Zhang, C., 2019. A multi-fault diagnostic method based on an interleaved voltage measurement topology for series connected battery packs. *Journal of Power Sources*, *417*, pp.132-144.

[11] Chen, Z., Xu, K., Wei, J. and Dong, G., 2019. Voltage fault detection for lithium-ion battery pack using local outlier factor. *Measurement*, *146*, pp.544-556.

[12] Pan, Y., Feng, X., Zhang, M., Han, X., Lu, L. and Ouyang, M., 2020. Internal short circuit detection for lithium-ion battery pack with parallel-series hybrid connections. *Journal of Cleaner Production*, *255*, p.120277.

[13] Raghavan, A., Kiesel, P., Sommer, L.W., Schwartz, J., Lochbaum, A., Hegyi, A., Schuh, A., Arakaki, K., Saha, B., Ganguli, A. and Kim, K.H., 2017. Embedded fiber-optic sensing for accurate internal monitoring of cell state in advanced battery management systems part 1: Cell embedding method and performance. *Journal of Power Sources*, *341*, pp.466-473.

[14] Li, B., Parekh, M.H., Adams, R.A., Adams, T.E., Love, C.T., Pol, V.G. and Tomar, V., 2019. Lithium-ion battery thermal safety by early internal detection, prediction and prevention. *Scientific reports*, *9*(1), p.13255.

[15] Said, A.O., Lee, C. and Stoliarov, S.I., 2020. Experimental investigation of cascading failure in 18650 lithium ion cell arrays: Impact of cathode chemistry. *Journal of Power Sources*, *446*, p.227347.

[16] Zou, K., Lu, S., Chen, X., Gao, E., Cao, Y. and Bi, Y., 2021. Thermal and gas characteristics of large-format LiNi0. 8Co0. 1Mn0. 1O2 pouch power cell during thermal runaway. *Journal of Energy Storage*, *39*, p.102609.

[17] Kennedy, R.W., Marr, K.C. and Ezekoye, O.A., 2021. Gas release rates and properties from Lithium Cobalt Oxide lithium ion battery arrays. *Journal of Power Sources*, *487*, p.229388.

[18] DENG, Z., HUANG, Z., LIU, L., HUANG, Y. and SHEN, Y., 2019. Applications of ultrasound technique in characterization of lithium-ion batteries. *Energy Storage Science and Technology*, *8*(6), p.1033.

[19] Appleberry, M.C., Kowalski, J.A., Africk, S.A., Mitchell, J., Ferree, T.C., Chang, V., Parekh, V., Xu, Z., Ye, Z., Whitacre, J.F. and Murphy, S.D., 2022. Avoiding thermal runaway in lithium-ion batteries using ultrasound detection of early failure mechanisms. *Journal of Power Sources*, *535*, p.231423.

[20] Su, T., Lyu, N., Zhao, Z., Wang, H. and Jin, Y., 2021. Safety warning of lithium-ion battery energy storage station via venting acoustic signal detection for grid application. *Journal of Energy Storage*, 38, p.102498.

[21] Lyu, N., Jin, Y., Miao, S., Xiong, R., Xu, H., Gao, J., Liu, H., Li, Y. and Han, X., 2021. Fault warning and location in battery energy storage systems via venting acoustic signal. IEEE Journal of Emerging and Selected Topics in Power Electronics, 11(1), pp.100-108.

[22] Tam, W.C., Chen, J., Fang, H., Tang, W., Deng, J. and Putorti Jr, A., 2025. Development of an early-stage thermal runaway detection model for lithium-ion batteries. *Journal of Power Sources*, *641*, p.236714.

[23] Wang, Q., Ping, P., Zhao, X., Chu, G., Sun, J. and Chen, C., 2012. Thermal runaway caused fire and explosion of lithium ion battery. *Journal of power sources*, *208*, pp.210-224.

[24] Mallick, S. and Gayen, D., 2023. Thermal behaviour and thermal runaway propagation in lithium-ion battery systems–A critical review. *Journal of Energy Storage*, *62*, p.106894.

[25] Hu, D., Huang, S., Wen, Z., Gu, X. and Lu, J., 2024. A review on thermal runaway warning technology for lithium-ion batteries. *Renewable and Sustainable Energy Reviews*, *206*, p.114882.

[26] Nie, B., Dong, Y. and Chang, L., 2024. The evolution of thermal runaway parameters of lithium-ion batteries under different abuse conditions: A review. *Journal of Energy Storage*, *96*, p.112624.

[27] Bugryniec, P.J., Resendiz, E.G., Nwophoke, S.M., Khanna, S., James, C. and Brown, S.F., 2024. Review of gas emissions from lithium-ion battery thermal runaway failure—Considering toxic and flammable compounds. *Journal of Energy Storage*, *87*, p.111288.

[28] Heiskanen, S.K., Kim, J. and Lucht, B.L., 2019. Generation and evolution of the solid electrolyte interphase of lithium-ion batteries. Joule, 3(10), pp.2322-2333.

[29] Adenusi, H., Chass, G.A., Passerini, S., Tian, K.V. and Chen, G., 2023. Lithium batteries and the solid electrolyte interphase (SEI)—progress and outlook. Advanced Energy Materials, 13(10), p.2203307.

[30] Hou, J., Yang, M., Wang, D. and Zhang, J., 2020. Fundamentals and challenges of lithium ion batteries at temperatures between− 40 and 60° C. Advanced Energy Materials, 10(18), p.1904152.

[31] Zheng, Y., Shi, Z., Ren, D., Chen, J., Liu, X., Feng, X., Wang, L., Han, X., Lu, L., He, X. and Ouyang, M., 2022. In-depth investigation of the exothermic reactions between lithiated graphite and electrolyte in lithium-ion battery. Journal of Energy Chemistry, 69, pp.593-600.

[32] Zhang, S.S., 2007. A review on the separators of liquid electrolyte Li-ion batteries. Journal of power sources, 164(1), pp.351-364.

[33] Wang, F., Ke, X., Shen, K., Zhu, L. and Yuan, C., 2022. A critical review on materials and fabrications of thermally stable separators for lithium-ion batteries. Advanced Materials Technologies, 7(5), p.2100772.

[34] Jung, S.K., Gwon, H., Hong, J., Park, K.Y., Seo, D.H., Kim, H., Hyun, J., Yang, W. and Kang, K., 2014. Understanding the degradation mechanisms of LiNi0. 5Co0. 2Mn0. 3O2 cathode material in lithium ion batteries. Advanced Energy Materials, 4(1), p.1300787.

[35] Rinkel, B.L., Vivek, J.P., Garcia-Araez, N. and Grey, C.P., 2022. Two electrolyte decomposition pathways at nickel-rich cathode surfaces in lithium-ion batteries. Energy & environmental science, 15(8), pp.3416-3438.

[36] Müller, M., Pfaffmann, L., Jaiser, S., Baunach, M., Trouillet, V., Scheiba, F., Scharfer, P., Schabel, W. and Bauer, W., 2017. Investigation of binder distribution in graphite anodes for lithium-ion batteries. Journal of Power Sources, 340, pp.1-5.

[37] Jiao, X., Yin, J., Xu, X., Wang, J., Liu, Y., Xiong, S., Zhang, Q. and Song, J., 2021. Highly energy-dissipative, fast self-healing binder for stable Si anode in lithium-ion batteries. Advanced Functional Materials, 31(3), p.2005699.

[38] Arbizzani, C., Gabrielli, G. and Mastragostino, M., 2011. Thermal stability and flammability of electrolytes for lithium-ion batteries. Journal of Power Sources, 196(10), pp.4801-4805.

[39] Deng, J., Yang, W., Zhang, Y., Pan, L., Kang, F., Ji, X. and Wu, H., 2025. Combustion characteristics and fire risk assessment of EC/DMC/EMC electrolytes for Li-ion batteries. Journal of Energy Storage, 110, p.115308.

[40] Liu, X., Stoliarov, S.I., Denlinger, M., Masias, A. and Snyder, K., 2015. Comprehensive calorimetry of the thermally-induced failure of a lithium ion battery. *Journal of Power Sources*, *280*, pp.516-525.

[41] Chen, H., Buston, J.E., Gill, J., Howard, D., Williams, R.C., Vendra, C.M.R., Shelke, A. and Wen, J.X., 2020. An experimental study on thermal runaway characteristics of lithium-ion batteries with high specific energy and prediction of heat release rate. *Journal of Power Sources*, *472*, p.228585.

[42] Yang, T., Yang, N., Zhang, X. and Li, G., 2016. Investigation of the thermal performance of axial-flow air cooling for the lithium-ion battery pack. *International Journal of Thermal Sciences*, *108*, pp.132-144.

[43] Wu, M.S., 2022. Multi-objective optimization of U-type air-cooled thermal management system for enhanced cooling behavior of lithium-ion battery pack. *Journal of Energy Storage*, *56*, p.106004.

[44] Liu, H., Wei, Z., He, W. and Zhao, J., 2017. Thermal issues about Li-ion batteries and recent progress in battery thermal management systems: A review. *Energy conversion and management*, *150*, pp.304-330.

[45] Regmi, P. and Wong, H., 2018. Heat and mass transfer in a cylindrical heat pipe with a circular-capillary wick under small imposed temperature differences. *International Journal of Heat and Mass Transfer*, *120*, pp.228-240.

[46] Liu, Q., Sun, C., Zhang, J., Shi, Q., Li, K., Yu, B., Xu, C. and Ju, X., 2023. The electro-thermal equalization behaviors of battery modules with immersion cooling. *Applied Energy*, *351*, p.121826.

[47] Liu, Q., Liu, Y., Zhang, M., Wang, S., Li, W., Zhu, X., Ju, X., Xu, C. and Wei, B., 2024. Comprehensive investigation of the electro-thermal performance and heat transfer mechanism of battery system under forced flow immersion cooling. *Energy*, *298*, p.131404.

Appendix A. Test Matrix for 18650 and 27100 Battery Experiments

Table A1 summarizes the complete test matrix for the 18650 NCA battery experiments. Experiments 1 - 14 correspond to the continuous heating tests, while Experiments 15 - 48 represent the interrupted heating tests. Experiments 18 - 20, 23, and 27 were intentionally excluded from analysis, as they were render-safe burns conducted solely to fully discharge and dismantle the batteries for post-test handling safety. In total, there are 43 experiments.

For the interrupted heating tests, the intervention time relative to the safety valve break (SVB) is color-coded for clarity: Blue cells indicate tests in which no ignition occurred after heating was stopped. Red cells indicate tests in which immediate ignition occurred. Uncolored cells represent cases of delayed ignition, where ignition occurred after an initial cooling or stabilization period.

Table A1. Summary of experiments for 18650 NCA Li-ion batteries.

	18650										
Experiment #	**Exp 1**	**Exp 2**	**Exp 3**	**Exp 4**	**Exp 5**	**Exp 6**	**Exp 7**	**Exp 8**	**Exp 9**	**Exp 10**	**Exp 11**
SOC (%)	100	100	100	100	75	75	75	75	50	50	50
Intervention Time Relative to SVB (s)	NA	NA	NA	NA	NA	NA	NA	NA	NA	NA	NA
Experiment #	**Exp 12**	**Exp 13**	**Exp 14**	**Exp 15**	**Exp 16**	**Exp 17**	**Exp 21**	**Exp 22**	**Exp 24**	**Exp 25**	**Exp 26**
SOC (%)	25	25	25	100	75	100	75	50	50	25	25
Intervention Time Relative to SVB (s)	NA	NA	NA	120	134	180	201	149	224	157	235
Experiment #	**Exp 28**	**Exp 29**	**Exp 30**	**Exp 31**	**Exp 32**	**Exp 33**	**Exp 34**	**Exp 35**	**Exp 36**	**Exp 37**	**Exp 38**
SOC (%)	100	100	75	50	25	25	50	25	100	100	75
Intervention Time Relative to SVB (s)	210	195	235	279	274	291	279	291	200	200	291
Experiment #	**Exp 39**	**Exp 40**	**Exp 41**	**Exp 42**	**Exp 43**	**Exp 44**	**Exp 45**	**Exp 46**	**Exp 47**	**Exp 48**	
SOC (%)	75	50	50	25	25	100	100	75	75	25	
Intervention Time Relative to SVB (s)	268	279	265	274	259	193	185	258	243	259	

Table A2 summarizes the complete test matrix for the 21700 NMC battery experiments. Experiments 49 - 60 correspond to the continuous heating tests, while Experiments 61 - 82 represent the interrupted heating tests. In total, there are 34 experiments.

For the interrupted heating tests, the intervention time relative to the safety valve break (SVB) is color-coded for clarity: Blue cells indicate tests in which no ignition occurred after heating was stopped. Red cells indicate tests in which immediate ignition occurred. Uncolored cells represent cases of delayed ignition, where ignition occurred after an initial cooling or stabilization period.

Table A2. Summary of experiments for 21700 NMC Li-ion batteries.

	21700										
Experiment #	**Exp 49**	**Exp 50**	**Exp 51**	**Exp 52**	**Exp 53**	**Exp 54**	**Exp 55**	**Exp 56**	**Exp 57**	**Exp 58**	**Exp 59**
SOC (%)	100	100	100	75	75	75	50	50	50	25	25
Intervention Time Relative to SVB (s)	NA	NA	NA	NA	NA	NA	NA	NA	NA	NA	NA
Experiment #	**Exp 60**	**Exp 61**	**Exp 62**	**Exp 63**	**Exp 64**	**Exp 65**	**Exp 66**	**Exp 67**	**Exp 68**	**Exp 69**	**Exp 70**
SOC (%)	25	100	100	75	75	50	50	25	100	100	75
Intervention Time Relative to SVB (s)	NA	43	33	48	37	30	40	50	20	20	25
Experiment #	**Exp 71**	**Exp 72**	**Exp 73**	**Exp 74**	**Exp 75**	**Exp 76**	**Exp 77**	**Exp 78**	**Exp 79**	**Exp 80**	**Exp 81**
SOC (%)	75	50	50	25	25	25	25	25	50	50	75
Intervention Time Relative to SVB (s)	25	40	40	65	101	89	89	100	50	50	12
Experiment #	**Exp 82**	**Exp19**	**Exp 20**								
SOC (%)	100	100	75								
Intervention Time Relative to SVB (s)	10	NA	NA								